FUNDAMENTAL PROPERTIES OF A NOVEL, METAL-DIELECTRIC, TUBULAR STRUCTURE WITH MAGNETIC RF COMPENSATION*

A. V. Smirnov†, RadiaBeam Systems, LLC, Santa Monica, CA 90404, USA
E. Savin, National Research Nuclear University (MEPhI), Moscow, 115409, Russia

Abstract

A number of electron beam vacuum devices such as small radiofrequency (RF) linear accelerators (linacs) and microwave traveling wave tubes (TWTs) utilize slow wave structures which are usually rather complicated in production and may require multi-step brazing and time consuming tuning. Fabrication of these devices becomes challenging at centimeter wavelengths, at large number of cells, and when a series or mass production of such structures is required. A hybrid, metal-dielectric, periodic structure for low gradient, low beam current applications is introduced here as a modification of Andreev's disk-and-washer (DaW) structure. Compensated type of coupling between even and odd TE01 modes in the novel structure results in negative group velocity with absolute values as high as 0.1c–0.2c demonstrated in simulations. Sensitivity to material imperfections and electrodynamic parameters of the disk-and-ring (DaR) structure are considered numerically using a single cell model.

INTRODUCTION

Industrial linac systems are employed in a wide variety of applications, from radiography to sterilization. In general, such a conventional system consists of standard, low-gradient, usually S-band, linac with beam energy from few to about ten MeVs, and average beam power in the range of few watts to 100 kW. As a rule these system are rather expensive, bulky, heavy, and not portable. The MicroLinac technology originally developed at SLAC [1] employs a compact X-band linear accelerator powered by an inexpensive, low power, pulsed magnetron [2,3]. However, to make the MicroLinac concept suitable for wider scope of applications, the conventional linac technology needs to be significantly advanced further to reduce cost, weight, and dimensions.

A biperiodic MicroLinac structure employs side [4] or on-axis [2] coupling cells enabling substantial bandwidth and number of cells to achieve beam energies exceeding 1 MeV within a single section at limited power supply (sub-MW in X-band). However, fabrication of a multi-cell, tapered MicroLinac structure remains rather expensive and time consuming. It requires significant efforts to machine the large number of different cells with very high precision. Besides, each cell usually needs to be cold-tested, some of the cells may require re-machining. A multi-step brazing is usually required along with individual tuning of the cells of the brazed assembly.

An attractive opportunity for eased fabrication of MicroLinac is using of dielectric loaded structures, in which a smooth ceramic-lined metal tube replaces the metal periodic structure [5,6,7]. However, a wide practical implementation of this approach is prevented by a number of problems. Among them are single-wall multipactor and charging of the dielectric material capable to damage the material at practical values of pulse repetition rates and beam currents. In a MicroLinac these problems are convoluted by substantial beam loss at finite capture of a usually continuous beam injected from a thermionic injector at low energies (a few tens of keV). An additional problem is a large spread of phase velocities required for a MicroLinac lying in the range of (0.3-1)c. Shunt impedance over Q of a dielectric loaded structure at low phase velocity is noticeably lower compared to a conventional π-mode, iris loaded structure. In addition that low phase velocity implies high permittivity for dielectrics (ε>20), which is usually associated with elevated loss factors and thus further reduction of shunt impedance.

One interesting modification of a conventional iris (or disk) loaded traveling wave structure is related to a hybrid dielectric and iris loaded periodic accelerating structure [8]. That modification enables remarkably low (approaching to unity) overvoltage (defined as a ratio of maximum surface field to peak accelerating field) at still substantial shunt impedance and group velocity. However, this modification does not take advantage of magnetic energy stored in the dielectric to provide magnetic coupling. A modified dielectric loaded, periodic structure has been introduced to enhance coupling impedance [9]. However, that dielectric-structured approach seems to be difficult to apply for fabrication of a long, multi-cell, strongly tapered MicroLinac. It may still suffer from the issues related to dielectric exposition to the beam and multipactor similar to that in conventional dielectric-loaded and iris-loaded hybrid structures.

A hybrid metal-dielectric, periodic slow-wave structure [10] enables higher group velocities, mitigation of the charging problem, and potential simplification of structure production for a low-current, low-gradient applications. In Fig. 1 we present a schematic of a single section X-band MicroLinac for radiography source replacement.

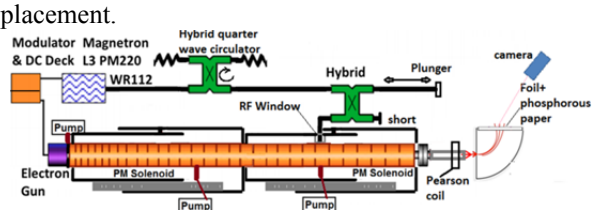

Figure 1: Schematic of a single section X-band MicroLinac system for radiography source replacement.

*Work supported by the U.S. Department of Energy (award No. DE-SC-FOA- SC0011370)
†asmirnov@radiabeam.com

DISK-AND-RING CELLS

Compensation of the Disk-and-Ring (DaR) cells is accomplished by making the same frequency for odd and even monopole modes as shown in Fig. 2 for high and low phase velocities. Unlike Andreev's disk-and-washer (DaW) structure [11] both modes are TM01.

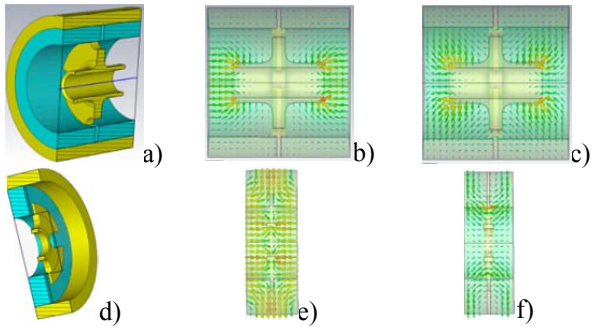

Figure 2: Cut view of compensated β_{ph}=0.94 (a-c) and β_{ph}=0.34 (d-f) X-band DaR cells with Alumina (a-c) and MgCaTiO3 (d-f) rings for even (b,e), and odd (c,f) modes. . Copper pipe internal diameter: ∅0.62".

In Fig. 3 and Fig. 4 we show frequency dispersion, shunt impedance, and Q-factor plotted as a function of phase advance per cell for the two modes resonant at θ=π phase advance at f=9.4 GHz±0.25MHz frequency.

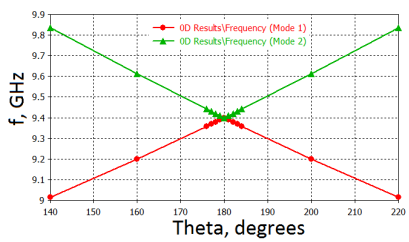

Figure 3: Two-mode Brillouin dispersion diagram for β_{ph}=0.94 DaR cell (ε=9.9 for the rings).

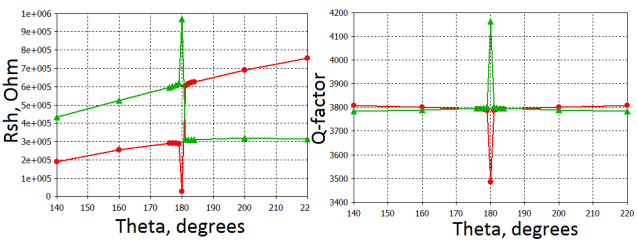

Figure 4: Shunt impedance (left) and Q-factor (right) as a function of phase advance for DaR cell of Fig. 2(a). Alumina high grade ceramic is used with ε=9.9 and tanδ=0.0001.

Next we applied a lower grade Alumina having dielectric constant ε=9.32 (instead of 9.9) to "detune" the cell of Fig. 2a. No structure geometry optimization or other change has been made for that variant. Simulation results are presented in Figs. 5, 6. In plots of Figs. 3, 5 one can select branches forming two smoothed dispersion curves corresponding also to smooth shunt impedance dependencies vs. phase advance (see Figs. 4,6). The "operating" curve can be composed from branches having highest shunt impedance. It dominates interaction with the beam. Both smoothed curves have an effective mode of operation corresponding to ~π/2 mode for the middle of phase advance range simulated. This is equivalent to presence of a resonant coupling cell because full 2π range for DaR structure appears as π range for a conventional structure having twice less period. .

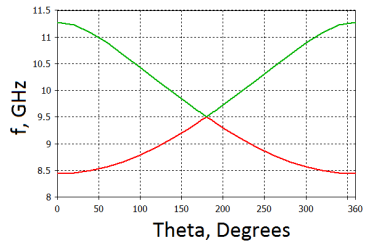

Figure 5: Two-mode Brillouin dispersion diagram for DaR cell of Fig. 2(a) at ε=9.32.

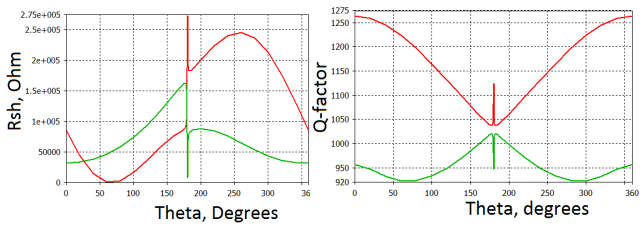

Figure 6: Shunt impedance (left) and Q-factor (right) as a function of phase advance for DaR cell of Fig. 2(a). Alumina low grade ceramic is used with ε=9.32 and tanδ=0.0019.

Therefore we can conclude that the DaR structure behaves phenomenologically as a biperiodic compensated structure. Thus interaction pattern with the beam at θ=π crossing did not change even at that significant 6% change in the dielectric constant compared to that of Fig. 6. That means the structure performance remains intact (i.e. compensated) and also indicates certain robustness in terms of dielectric constant deviations and fabrication errors.

MULTI-CELL STRUCTURE DESIGN

We found that the normalized group velocity β_{gr} varies from -0.19 to -0.1 for β_{ph}=0.34-0.94 at the f=9.4 GHz. That indicates strong magnetic coupling and hence great opportunity for multi-cell performance of the assembly employed as a standing wave (SW) linac.

We have studied a shorter (vs. 44-cells version [10]) assembly shown in Fig. 7 with vacuum ports (on the bottom) and RF port (on the top). Our multi-cell MicroLinac DaR structures include a few non-compensated, π-mode, low-β_{ph} DaR cells.

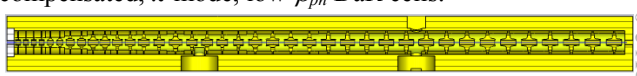

Figure 7: 39-cell, 0.42 m long, DaR MicroLinac section.

In Fig. 8 we simulated field profiles along the structure with rings made from different materials. Typical frequency separation between adjacent modes is ~50 MHz or higher. Note field profiles and the resonant

frequency are affected by significant difference in sensitivity to meshing for different cells. That may easily lead to numerically unstable results or poor convergence.

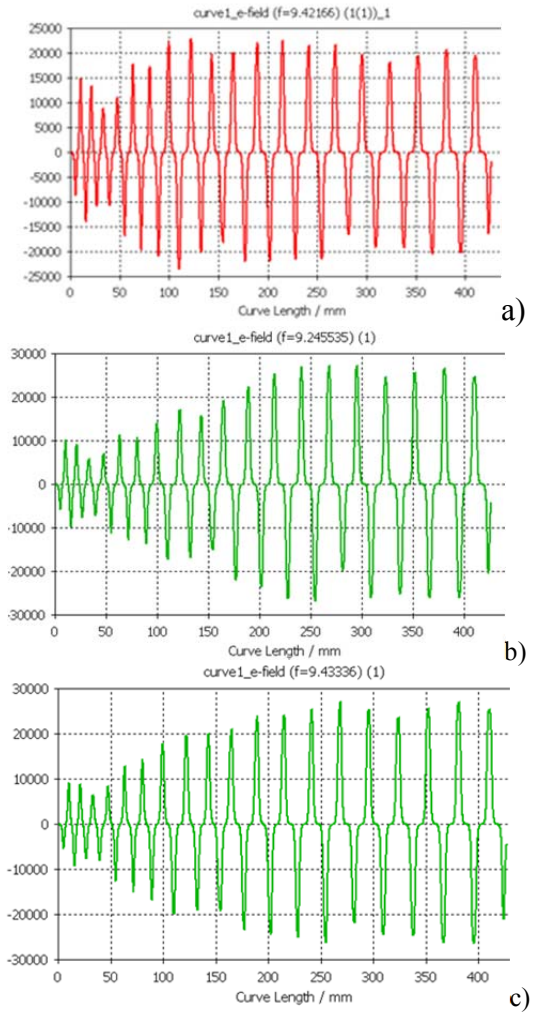

Figure 8: Longitudinal electric field profiles simulated along DaR section of Fig. 7 for ε=9.9 (a), and Sapphire with longitudinal (b) and transverse (c) C-axis orientation.

BEAM DYNAMICS

We applied the same solenoidal type focusing implemented with permanent magnet blocks used in prior MicroLinac designs [4]. ASTRA [12] simulation results are shown in Figs. 9, 10 for setups of Fig. 8a,b respectively and total RF power <200 kW.

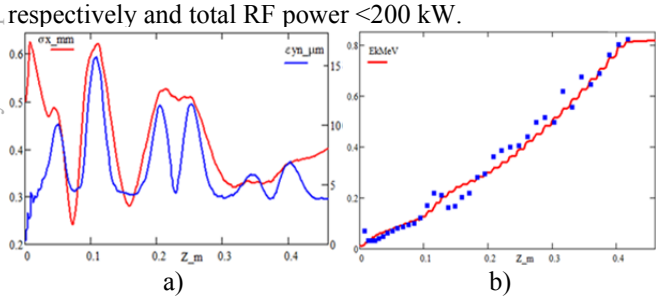

Figure 9: Beam rms transverse size [mm], emittance [μm] (a), and energy [MeV] (b) along section of Fig. 8a. Capture coefficient for 14 keV beam is ~20%. Maximum Ez field magnitude along the structure is 11.5 MV/m.

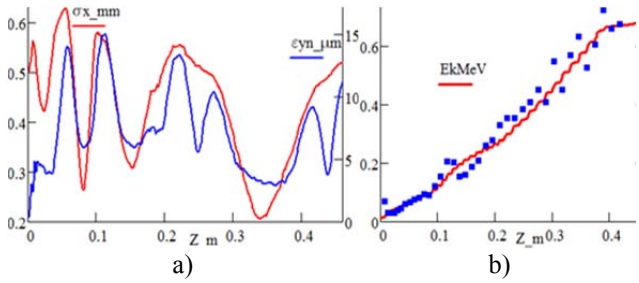

Figure 10: Beam rms transverse size [mm], emittance [μm] (a), and energy [MeV] (b) along section of Fig. 8b. Capture coefficient for 14 keV beam is ~9%. Blue squares correspond to energies at β_{ph} extracted from Fig. 8b. Maximum Ez field magnitude is 14 MV/m.

Thus DaR structure is rather tolerable to deviations of dielectric properties and/or geometry. That feature suggests elimination of tuning of the individual cells.

REFERENCES

[1] N. Ackerman *et al.*, "MicroLinac – A Portable Accelerator for Radiography," The 12th Advanced Accelerator Concepts Workshop, 2006.

[2] T. Yamamoto, T. Natsui, F. Sakamoto, M. Uesaka, N. Nakamura and E. Tanabe, "Development of portable X-band linac X-ray source for non-destructive testing," Proceedings of the Joint International Workshop: Nuclear Technology and Society–Needs for Next Generation, Berkeley, California, 2008.

[3] S. Boucher, X. Ding, A. Murokh, in *Proc. of IPAC'10*, Kyoto, Japan, 2010, p. 178.

[4] S. Boucher, R. Agustsson, L. Faillace, J. Hartzell, A. Murokh, A. Smirnov, S. Storms, K. Woods. In *Proc. of IPAC2013*, Shanghai, China, 2013, p. 3746.

[5] E. Chojnacki *et al.*, *J. Appl. Phys.*, vol. 69, p. 6257, 1991.

[6] P. Zou *et al.*, *Rev. Sci. Instrum.* Vol. 71, pp. 2301–2304, 2000.

[7] C. Jing, J. G. Power, *et al.*, in *Proc. of PAC'05*, Knoxville, Tennessee, 2005, pp. 1566-1569.

[8] P. Zou, L. Xiao, X. Sun, W. Gai. In *Proc. of PAC2001*, p 3966.

[9] D. Satoh, M. Yoshida, N. Hayashizaki. *Phys. Rev. Accelerators and Beams, vol.* 19, p. 011302, 2016.

[10] A. V. Smirnov, S. Boucher, S. Kutsaev, R. Agustsson, R. Berry, K. Junge, J. Hartzell, J. McNevin, A. Murokh, E. Savin, G. Leyh, in *Proc. of IPAC2016*, Busan, Korea, p. 1992.

[11] V. G. Andreev *et al.*, *Soviet Physics - Technical Physics,* vol 13, p. 1070, 1969.

[12] "Astra - A space charge tracking algorithm. User's manual." Version 3.1, DESY, Hamburg, 2014; http://www.desy.de/~mpyflo/Astra_manual/Astra-Manual_V3.1.pdf